Petroleum 1 (2015) 118–132

Contents lists available at ScienceDirect

Petroleum

journal homepage: www.keaipublishing.com/en/journals/petlm

Original article

Determination of oil well production performance using artificial neural network (ANN) linked to the particle swarm optimization (PSO) tool

Mohammad Ali Ahmadi [a], Reza Soleimani [b], Moonyong Lee [c], Tomoaki Kashiwao [d], Alireza Bahadori [e, *]

[a] Department of Petroleum Engineering, Ahwaz Faculty of Petroleum Engineering, Petroleum University of Technology, Ahwaz, Iran
[b] Young Researchers and Elite Club, Neyshabur Branch, Islamic Azad University, Neyshabur, Iran
[c] School of Chemical Engineering, Yeungnam University, Gyeungsan, Republic of Korea
[d] Department of Electronics and Control Engineering, National Institute of Technology, Niihama College, 7-1 Yagumo-cho, Niihama, Ehime 792-8580, Japan
[e] School of Environment, Science & Engineering, Southern Cross University, Lismore, NSW, Australia

ARTICLE INFO

Article history:
Received 15 May 2015
Received in revised form
6 June 2015
Accepted 8 June 2015

Keywords:
Well productivity
Drainage area
Skin factor
Least square Support vector machine
Hybrid connectionist model
Particle swarm optimization

ABSTRACT

Greater complexity is involved in the transient pressure analysis of horizontal oil wells in contrast to vertical wells, as the horizontal wells are considered entirely horizontal and parallel with the top and underneath boundaries of the oil reserve. Therefore, there is an essential need to estimate productivity of horizontal wells accurately to examine the effectiveness of a horizontal well in terms of technical and economic prospects.

In this work, novel and rigorous methods based on two different types of intelligent approaches including the artificial neural network (ANN) linked to the particle swarm optimization (PSO) tool are developed to precisely forecast the productivity of horizontal wells under pseudo-steady-state conditions. It was found that there is very good match between the modeling output and the real data taken from the literature, so that a very low average absolute error percentage is attained (e.g., <0.82%). The developed techniques can be also incorporated in the numerical reservoir simulation packages for the purpose of accuracy improvement as well as better parametric sensitivity analysis.

1. Introduction

Petroleum engineers are always interested in finding appropriate and reliable tools to predict the productivity of horizontal well as accurate predictions seem very important to conduct technical and economical feasible studies before drilling the wells which is very costly. It is a very important factor to decide on the economical feasibility of drilling horizontal wells [1–7].

According to the experimental investigation conducted by Yasar et al. [8]; applied load and torque for both specific energy and penetration rate in drilling operations have great importance. Based on their results, penetration rate decreases dramatically with raising Unconfined Compressive Strength (UCS) of the cement grout being drilled, proposing that rock characters will intensely effect advance in the drilling operation, and determined specific energy decreases dramatically with both raising applied load and raising penetration rate in the drilling operation [8]. Moreover, Wasantha et al. [9] studied the effect of strain rate on the mechanical behavior of sandstones with various grain sizes. They concluded that size of constituent grains is an essential factor which requires to be encompassed in

* Corresponding author.
E-mail addresses: ahmadi6776@yahoo.com (M.A. Ahmadi), alireza.bahadori@scu.edu.au (A. Bahadori).

Peer review under responsibility of Southwest Petroleum University.

Production and Hosting by Elsevier on behalf of KeAi

http://dx.doi.org/10.1016/j.petlm.2015.06.004

thoughts of the mechanical behavior of sandstones under various strain rates [9].

The pseudo-steady state occurs when the fluid production manifests its impact in the boundaries far from the production well where the oil is approaching from the drainage boundary on the way to the depletion area around the well [10,11].

It indicates that the reservoir has reached a condition where the pressure at all reservoir boundaries and also the average reservoir pressure will reduce over time as more fluid is extracted from the reservoir [12,13].

A suitable technique to estimate the pressure transient response of producing horizontal wells was developed by Clonts and Ramey [14]; where the source functions are combined with the Newman product approach. Recently, an analytical approach was also introduced by Hagoort [15] to calculate the productivity of a horizontal well with infinite conductivity placed in a reservoir which is considered as a closed rectangular system.

The resultant of the source functions was utilized by Daviau et al. [16] for oil reservoirs with particular characteristics. A reliable solution was presented by Ozkan et al. [17] and Joshi [18] to estimate pressure response for the anisotropic and infinite reservoirs which experience either uniform influx or include a horizontal well with infinite-conductivity.

Several researchers performed a variety of works to use the source function scheme to obtain profile or/and magnitudes of pressure in surrounded reservoirs [16,4,5,19,20,7,21].

The horizontal well-bore was considered as a strip source by Goode and Thambynayagam [22]. In their work a uniform distribution of flow rate in the well length is maintained. The pressure response was found for the horizontal producing well through combination of the finite Fourier cosine and Laplace transforms.

Depletion mode, especially in linear flow patterns depends on well productivity in non-circular flow configurations. Helmy and Wattenbarger [23] noticed that this observation matches well with the analytical long-time solutions for the analogous linear heat flow problems.

In general, the horizontal wells are not fully drilled in horizontal direction such that a significant change in vertical elevation happens during the drilling, leading to huge effects on outlet pressure of the horizontal well. In addition, the computation usually is difficult due to negative skin factor of horizontal wells. On the other hand, accurate calculation of the length of horizontal production well is not simple in many cases [2].

Production at a constant well rate plays a major role in current analytical approaches to study the productivity of horizontal wells in closed reservoirs [24,25].

Helmy and Wattenbarger [26] presented simple productivity correlations using several number of reservoir simulations to calculate the productivity of horizontal wells. The reservoir model contained a homogeneous, isotropic, closed reservoir with the shape of a rectangular box and an open hole horizontal well parallel to one of the sides of the box.

A semi-analytical model to determine of the productivity of wells in Darcy flow systems was presented by Hagoort [27].

Finally, summary of the productivity models in steady state and pseudo-steady state conditions is demonstrated in Table 1. It should be noted that, each of equations should only use in the specific circumstances. In other words, various assumptions should be met to use each correlations (for instance, steady state flow regime, homogeneous porous media and etc) and this is a big disadvantage for petroleum engineers to employ the aforementioned correlations. Moreover, most of the correlations developed are depending on the size of the system because they are not dimensionless and this is another drawback for using these formulas.

An attempt was made by Mutalik et al. [28] to compile different data sets of shape factors and the corresponding skin factors (S_{CAh}), where different horizontal wells are considered at various locations of the drainage area in the reservoir [2]. The presence of an enclosed reservoir and an infinite-conductivity well are the main assumptions in their methodology. The horizontal well productivity is determined by an equation as given below [2]:

$$J_h = \frac{q_o}{P_R - P_{wf}} = \frac{kh}{141.2\beta_o\mu_o}\left(\frac{1}{\ln\left(\frac{r'_e}{r_w}\right) - A' + S_f + S_m + S_{CAh} - C' + Dq_o}\right) \quad (1)$$

where

$$r'_e = \sqrt{\frac{A}{\pi}} \quad (2)$$

$$S_f = -\ln\left[\frac{L}{4r_w}\right] \quad (3)$$

Bahadori et al. [29] introduced a predictive tool buy means of Vandermonde matrix concepts, for estimating pseudo skin factor of horizontal wells through rectangular drainage area. They noticed that the calculation of productivity of a horizontal oil well depends on the pseudo-skin factor for centrally located wells within different drainage areas.

Given the above matters, developing a proper and straightforward correlation seems necessary. Compared to available approaches, the developed equation is expected to be less complicated, and more accurate for predicting the pseudo-skin factor as a function of dimensionless length (L_D) and the ratio of horizontal well length over drainage area side ($L/2X_e$) for square and rectangular shapes with ratios of sides 1, 2, and 5.

$$L_D = \frac{L}{2h}\sqrt{\frac{K_v}{K_h}} \quad (4)$$

In this article, an intelligent method utilizing a new type of network modeling which called “Least Square Support Vector Machine (LSSVM)” is developed to serve as a rapid and inexpensive predictive model for monitoring well productivity of horizontal wells in box shape drainage area. The proposed LSSVM model is developed implementing extensive actual well productivity data.

To depict the robustness, integrity and accuracy of the suggested LSSVM model, the obtained outcomes from the introduced approach are contrasted with the relevant actual productivity data. Outputs from this research reveal that the evolved approach can monitor the horizontal well productivity with high accuracy. The introduced predictive model can be utilized as a reliable way for quick and cheap but efficient prediction of well productivity of horizontal well parameter in absence of appropriate experimental or/and real data, specifically through the initial stages of evolvement of horizontal well drilling.

Table 1
Summary of previous productivity equations.

Joshi-steady state [18]	$q_o = \frac{k_H h(p_e - p_{wf})}{141.2\mu_o B_o \left\{ \ln\left[\frac{a+\sqrt{a^2-\left(\frac{L}{2}\right)^2}}{L/2}\right] + \frac{I_{ani}h}{L}\left(\ln\left[\frac{I_{ani}h}{r_w(I_{ani}+1)}\right]+s\right)\right\}}$
Butler-steady state [30]	$q_o = \frac{7.08\times10^{-3}k_H L(p_e-p_{wf})}{\mu_o B_o\left[I_{ani}\ln\left[\frac{hI_{ani}}{r_w(I_{ani}+1)}\right]+\frac{y_b\pi}{h}-1.14I_{ani}+s\right]}$
Furui et al.-steady state [10]	$q_o = \frac{7.08\times10^{-3}k_H L(p_e-p_{wf})}{\mu_o B_o\left[\ln\left[\frac{hI_{ani}}{r_w(I_{ani}+1)}\right]+\frac{y_b\pi}{hI_{ani}}-1.224+s\right]}$
Joshi-pseudo steady state [18]	$q_o = \frac{\sqrt{k_x k_z}b(\overline{p}-p_{wf})}{141.2\mu_o B_o\left\{\ln\left[\frac{\sqrt{A}}{r_w}\right]+\ln C_H - 0.75+s+s_R\right\}}$
	$\ln C_H = 6.28\frac{a}{I_{ani}h}\left[\frac{1}{3}-\frac{x_o}{a}+\left(\frac{x_o}{a}\right)^2\right]-\ln\left(\sin\frac{\pi z_o}{h}\right)-\frac{1}{2}\ln\left(\frac{a}{I_{ani}h}\right)-1.088$
First radial [31]	$q_o = \frac{2\sqrt{k_H k_V}L_{1/2}(p_i-p_{wf})}{162.6\mu_o B_o\left[\log\left[\frac{\sqrt{k_H k_V}t}{\varnothing r_w C_t r_w^2}\right]-3.2275+0.8686s-2\log\frac{1}{2}\left(\sqrt[4]{\frac{k_H}{k_V}}+\sqrt[4]{\frac{k_V}{k_H}}\right)\right]}$
	$t \le \frac{\varphi\mu_o C_t}{0.0002637\pi k_V}\min\{z_w^2,(h-z_w)^2\}$
Second radial [31]	$q_o = \frac{\sqrt{k_H k_V}L_{1/2}(p_i-p_{wf})}{162.6\mu_o B_o\left[\log\left[\frac{\sqrt{k_H k_V}t}{\varnothing r_w C_t r_w^2}\right]-3.2275+0.4343s-\log\left[\left(1+\sqrt{\frac{k_V}{k_H}}\right)\frac{z_w}{r_w}\right]\right]}$
	$\frac{\varphi\mu_o C_t}{0.0002637\pi k_V}\min\{z_w^2,(h-z_w)^2\} \le t \le \frac{\varphi\mu_o C_t}{0.0002637\pi k_V}\max\{z_w^2,(h-z_w)^2\}$
Intermittent time-linear [31]	$q_o = \frac{(p_i-p_{wf})}{B_o\left[\frac{8.128}{2hL_f}\sqrt{\frac{\mu_o t}{\varnothing k_H C_t}}+\frac{141.2\mu_o}{k_h h}s_z+\frac{70.6\mu_o}{L_f\sqrt{k_H k_V}}s\right]}$
	$s_z = -1.1513\sqrt{\frac{k_H}{k_V}}\frac{h}{L_f}\log\left[\frac{\pi r_w}{h}\left(1+\sqrt{\frac{k_V}{k_H}}\right)\sin\left(\frac{\pi z_w}{h}\right)\right]$
	$\frac{\varphi\mu_o C_t h^2}{0.0002637\pi k_V} \le t \le \frac{\varphi\mu_o C_t L_{f/2}^2}{0.0002637\pi k_V}$
Late time-radial [31]	$q_o = \frac{(p_i-p_{wf})}{\mu_o B_o\left[\frac{162.6}{k_h h}\left[\log\left[\frac{\sqrt{k_H k_V}t}{\varnothing r_w C_t r_w^2}\right]\right]+\frac{141.2\mu_o}{k_h h}s_z+\frac{70.6\mu_o}{L_f\sqrt{k_H k_V}}s\right]}$
	$t \ge \frac{\varphi\mu_o C_t L_{f/2}^2}{0.0002637\pi k_V}$
	$s_z = -1.1513\sqrt{\frac{k_H}{k_V}}\frac{h}{L_f}\log\left[\frac{\pi r_w}{h}\left(1+\sqrt{\frac{k_V}{k_H}}\right)\sin\left(\frac{\pi z_w}{h}\right)\right]-0.5\frac{k_H}{k_V}\frac{h^2}{L_f^2}\left(\frac{1}{3}-\frac{z_w}{h}+\frac{z_w^2}{h^2}\right)$

2. Description of physical model

Fig. 1 illustrates the schematic of the horizontal well configuration which is characterized by the straightforward analytical approach: a cubic reservoir with a horizontal well parallel to the top and bottom of the cube. The reservoir has a width w and thickness h and length $2X_e$. An open hole horizontal well with a length of L is assumed drilled in the box shaped reservoir.

The location of the drilled well is determined by three points which demonstrate the Cartesian coordinates such as x_w, y_w and z_w. It should be noted that the Cartesian coordinates of the midpoint of the horizontal well throughout the Cartesian system which is tier collateral to the edges of the cubic reservoir. Moreover, direction of the horizontal well is parallel to the x-axis of Cartesian coordinate system. The aforementioned reservoir is isotropic and homogeneous and consists a compressible fluid with a constant compressibility and constant viscosity. No flow boundaries are assumed for the outer boundaries of the reservoir. Production from well may be at constant pressure or constant rate. Well conductivity in aforementioned reservoir is consumed infinite, which conveys pressure distribution throughout the wellbore is uniform.

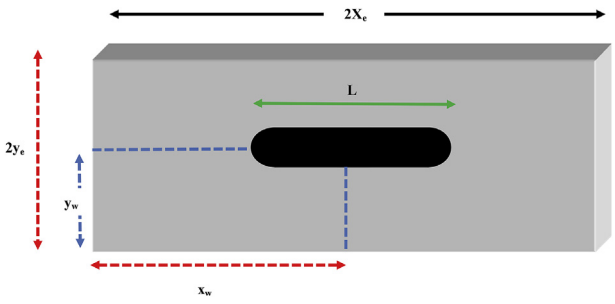

Fig. 1. The schematic of the horizontal well in the box-shaped drainage area.

The 2D flow configuration of horizontal well in the abovementioned system is depicted in Fig. 2. As clear be seen in this figure, two types of flow exist in horizontal wells including horizontal flow to a fully penetrating vertical fracture with length L_w, and the flow to a fully penetrating horizontal well in a rectangular reservoir of thickness h.

3. Methodology

3.1. Artificial neural network

The artificial neural networks (ANNs) have been built on the basis of function and configuration of the brain of human, nerve networks, and complicated procedure of learning and reacting. It

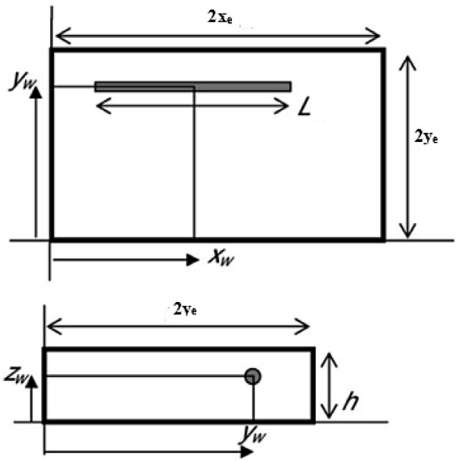

Fig. 2. Vertical and horizontal well configuration.

aims to produce the magnitudes of target parameters from input information through internal computations and analysis. In general, this connectionist technique involves well interconnections model along with a simple processing constituent (or neuron) that is able to find out the right links between independent and dependent parameters. The multilayer feed forward neural network is the most common and acceptable ANN system, where the neurons are coordinated into different layers; namely, input, output, and hidden.

Multilayer feed forward neural networks usually have one or more hidden layers, which enable the networks to model non-linear and complex functions. The hidden layer is responsible to convey meaningful information between the input and network stages through an effective approach. ANNs interface predictors through the neurons of an input layer and transmit output of dependent variable(s) through the neurons of an output layer. Each neuron in hidden and output layers carries a transfer function that illustrates internal activation phenomenon. A neuron output is normally achieved through transformation of its input employing an opposite transfer function.

Transfer functions may be linear or non-linear. It should be mentioned that, each interconnection in an ANN has a strength that is expressed by a number referred to as weight. Furthermore, bias is an extra input appended to neurons, and which all the time holds a value of 1 and treated similar to other weights [32]. Fig. 3 illustrates the structure of a feed forward ANN with one hidden layer used in this study.

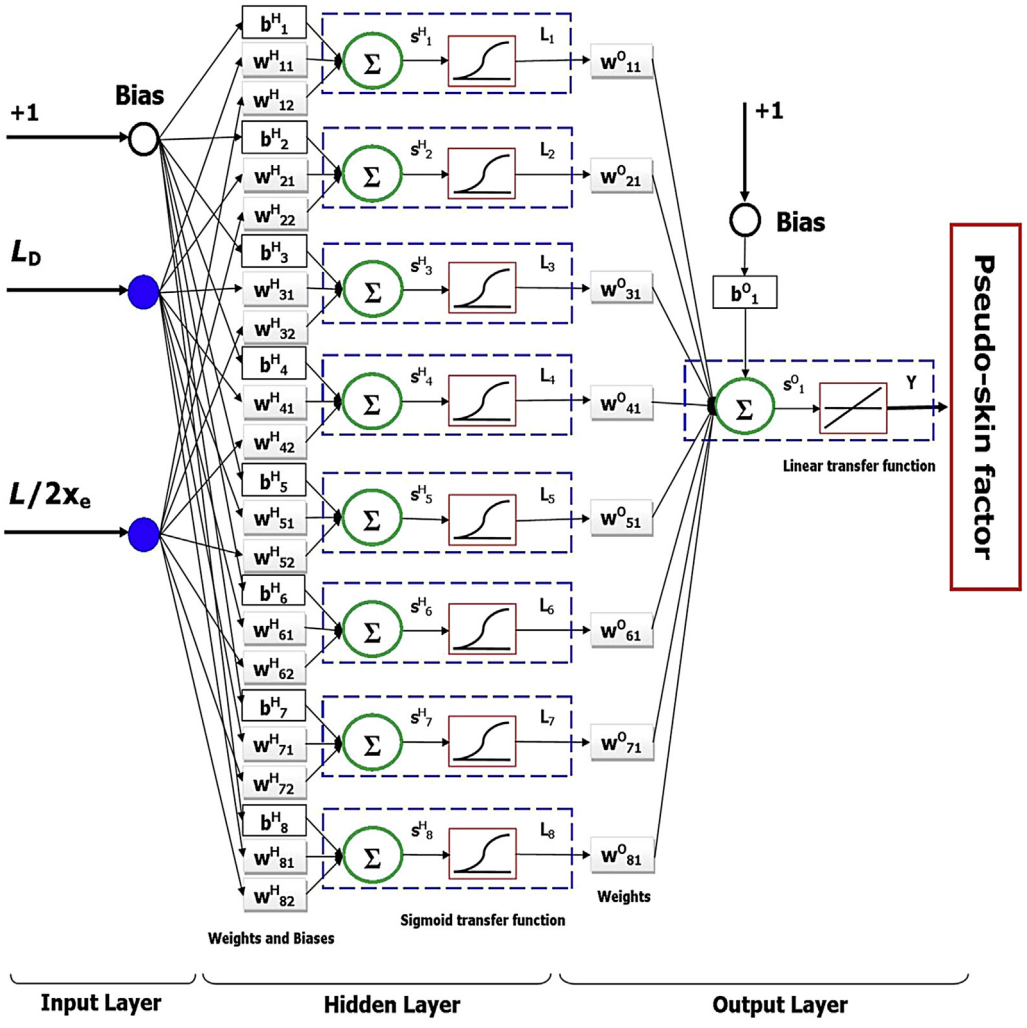

Fig. 3. Structure of the proposed three layer feed forward neural network model.

A brief procedures to produce the output variable, using the input data, are described below. Given the info for inputs neurons, the net inputs (S) for the hidden neurons are computed as follows:

$$S_j^{\mathrm{H}} = \sum_{t=1}^{2} w_{j,t}^{\mathrm{H}} \cdot a_t + b_j^{\mathrm{H}} \tag{5}$$

where a_t is the vector of the input parameters, j is the index of hidden neuron, $w_{j,t}^{\mathrm{H}}$ denotes the interconnection weight between the input neurons with the hidden layer, and the term b_j^{H} stands for the bias of the jth hidden neuron. Then, the outputs (L_j) of the hidden neurons are computed, utilizing a transfer function f_{H} which is associated with the hidden neurons.

$$L_j = f_{\mathrm{H}}\left(S_j^{\mathrm{H}}\right) = f_{\mathrm{H}}\left(\sum_{t=1}^{2} w_{j,t}^{\mathrm{H}} \cdot a_t + b_j^{\mathrm{H}}\right) \tag{6}$$

The produced outputs from the hidden layer are presented to the output layer as inputs. The output of the output layer (the final output, Y) can be also calculated in similar way. Indeed, it is responsibility of all neurons in a network to relate the input information to the desired output function through an adequate and suitable correlation.

3.2. Least squares support vector machines

Support vector machine (SVM) is a new kind of learning machine which was developed within the context of statistical learning theory and structural risk minimization by Vapnik and his colleagues [33–36,37–41]. SVM is a very nice methodology which has recently attracted special attention from a great deal of researchers for solving problems in nonlinear classification, function estimation as well as for solving density estimation problems [42,33–36,37–41], due to it enjoys several interesting properties such as the use of the kernel-induced feature spaces, the sparseness of the solution, high generalization ability, together with excellent performance.

An evolved version of SVM, called LSSVM was recently introduced by Suykens and co-workers in which the inequality constraints of an SVM were changed into a set of equality constraints, in order to facilitate the original SVM method [33–36,37–41,53,44]. Therefore, the solution is obtained by solving a system of linear equations, resulting in an easier-to-implement and faster alternative to the original SVM method [45–48,43,44]. It should be mentioned that, this section of the paper serves as an overview to LSSVM. Details of this method can be found in the literature [33–36,37–41,49,43,44].

Assume a set of N training data $\{(x_1, y_1), (x_2, y_2), \ldots, (x_N, y_N)\}$, where $x_k \in \mathbb{R}^n$ is the kth input data and $y_k \in \mathbb{R}$ is corresponding output value. The aim is to estimate a model of the formula [33–36,37–41]:

$$y(x) = \mathscr{W}^{\mathrm{T}} \varphi(x) + b \tag{7}$$

where $\varphi(\cdot) : \mathbb{R}^n \to \mathbb{R}^{n_h}$ is a nonlinear mapping function, which maps the input data to higher dimensional feature space; b is the bias term and $\mathscr{W}$ denotes the weight vector needed to be determined, which can be calculated by minimizing the following function [33–36,37–41]:

$$\mathscr{J}(\mathscr{W}, e) = \frac{1}{2}\mathscr{W}^{\mathrm{T}}\mathscr{W} + \frac{1}{2}\gamma \sum_{k=1}^{N} e_k^2 \tag{8}$$

Subject to the following equality constraint [33–36,37–41]:

$$y_k = \mathscr{W}^{\mathrm{T}} \varphi(x_k) + b + e_k, \quad k = 1, 2, \ldots, N \tag{9}$$

where γ is the regularization constant used for preventing over fitting, and e_k is the training data error. After then, the Lagrangian function is adopted as follow in order to solve the constrained optimization problem [33–36,37–41]:

$$\mathscr{L}(\mathscr{W}, b, e, \alpha) = \mathscr{J}(\mathscr{W}, e) - \sum_{k=1}^{N} \alpha_k \left\{ \mathscr{W}^{\mathrm{T}} \varphi(x_k) + b + e_k - y_k \right\} \tag{10}$$

where α_k are Lagrange multipliers. By executing the first order partial derivatives of Lagrange function (8) with respect to $\mathscr{W}, b, e_k$ and α_k the conditions for optimality can be written as follow [33–36,37–41]:

$$\partial_{\mathscr{W}} \mathscr{L} = \mathscr{W} - \sum_{k=1}^{N} \alpha_k \varphi(x_k) = 0 \tag{11}$$

$$\partial_b \mathscr{L} = \sum_{k=1}^{N} \alpha_k = 0 \tag{12}$$

$$\partial_{e_k} \mathscr{L} = \alpha_k - \gamma e_k = 0, \quad k = 1, \ldots, N \tag{13}$$

$$\partial_{\alpha_k} \mathscr{L} = \varphi(x_k) \cdot \mathscr{W}^{\mathrm{T}} + b + e_k - y_k = 0, \quad k = 1, \ldots, N \tag{14}$$

When the variables $\mathscr{W}$ and e are removed, the optimization problems can be described as a linear system [33–36,37–41].

$$\begin{bmatrix} 0 & 1_v^{\mathrm{T}} \\ 1_v & \Omega + \gamma^{-1} I \end{bmatrix} \begin{bmatrix} b \\ \alpha \end{bmatrix} = \begin{bmatrix} 0 \\ y \end{bmatrix} \tag{15}$$

where $y = [y_1 \ldots y_N]^{\mathrm{T}}$, $1_v = [1 \ldots 1]^{\mathrm{T}}$, $\alpha = [\alpha_1 \ldots \alpha_N]^{\mathrm{T}}$, I is an identity matrix and Ω is an N-dimensional symmetric matrix; $\Omega_{kl} = \varphi(x_k)^{\mathrm{T}} \cdot \varphi(x_l) = K(x_k, x_l), \quad \forall k, l = 1, \ldots, N$. $K(x_k, x_l)$ is the kernel function and must meet Mercer's theorem. The resulting formulation of LSSVM model for function estimation is represented as [33–36,37–41]:

$$y(x) = \sum_{k=1}^{N} \alpha_k K(x, x_k) + b \tag{16}$$

where (b, α) is the solution to the linear system (15).

4. Developed models

In the current research, we applied two types of artificial intelligence based methodologies, viz. ANN and LSSVM to build the predictive models to calculate the shape-related skin factor or pseudo-skin factor in horizontal wells as a function of dimensionless length and the ratio of horizontal well length over drainage area side for various drainage areas based on previously published database [2,28].

4.1. ANN model

4.1.1. Data distribution (training and testing subsets)

When training multilayer feed-forward neural networks, the general practice is to first separate the data into two subsets [45]. The first subset is the training set, which is used for updating the

network weights and biases. The accuracy of trained neural network can be independently measured by the second data subset called testing set.

This will give us a sense of how well the network will do when applied to data from the real world. Herein, total of 96 data points (80% of whole data set) were used as training data and main data set were considered as a test data.

4.1.2. Training method and transfer functions

A key consideration in ANN design is the type of transfer functions. Different transfer functions can be used for neurons in the hidden and output layers. Among different transfer functions available, the log-sigmoid transfer function (logsig), which is an appropriate choice for many nonlinear functions, was employed as the transfer function for neurons in hidden layer which is mathematically expressed as:

$$f(S) = \frac{1}{1+\exp(-S)} \tag{17}$$

The logsig function is bounded between 0 and 1. One of the most remarkable features of this transfer function lies in its S shape which provides appropriate gain for a wide range of input levels. It should be mentioned that, ANNs be indebted their non-linear ability to exploit such non-linear transfer functions [50].

Also, for output layer, linear transfer function (purelin) is applied as a transfer function which is represented as:

$$f(S) = S \tag{18}$$

Outputs in the range of $-\infty$ to $+\infty$, can be produced from the linear transfer function [50].

ANNs' ability to deal with problems successfully greatly depends on applying an appropriate and effective training algorithm. Training process is basically an optimization process by which the weights of interconnections between neurons together with the biases are adjusted so that the network can predict the correct outputs for a given set of inputs.

There are many different types of training algorithms which have been applied for various applications such as Back Propagation (BP) [45], Genetic Algorithm (GA) [51], Particle Swarm Optimization (PSO) [47,52,50,53], Hybrid Genetic Algorithm and Particle Swarm Optimization (HGAPSO) [54,55], Unified Particle Swarm Optimization (UPSO) [56] and Imperialist Competitive Algorithm (ICA) [57,58].

In this study, PSO algorithm was implemented as a training algorithm for updating the weights and biases of multilayer feed forward network based on success stories of this new evolutionary computation algorithm for training ANNs in addition to its outstanding features including robustness, simplicity, flexibility, superior convergence characteristics and many others.

PSO is a population-based optimization algorithm based on the simulation of the social behavior of bird flocks, fish schooling and swarm of insects developed by [59], where the system is randomly initialized with a swarm of particles (potential solutions) and then searches the optima within the search space through updating generations. Particles inside the swarm are drawn progressively towards the global optimum as the system iterates. In each iteration, each particle knows and stores the two best values. The earliest value is the personal best position $p_{i,p_{\text{best}}}$ that is the location of the particle i in the search space, where it has attained the preeminent solution up to now, based on the fitness function. The global best solution $p_{g_{\text{best}}}$ is taken into account as the second one that introduces a position, leading to the best solution among all the particles on the same basis. Using this information, the velocity and position of each particle are updated according to the following formulae and consequently the new swarm of particles is generated with improved characteristics:

$$v_i^{n+1} = \omega v_i^n + c_1 r_1^n \left[p_{i,p_{\text{best}}}^n - p_i^n\right] + c_2 r_2^n \left[p_{g_{\text{best}}}^n - p_i^n\right] \tag{19}$$

$$p_i^{n+1} = p_i^n + v_i^{n+1} \tag{20}$$

where v_i^n and v_i^{n+1} are velocities of particle i at iterations n and $n+1$; p_i^n and p_i^{n+1} are positions of particle i at iterations n and $n+1$; ω is the inertia weight that plays an important role to handle the exploration and exploitation of the search space, as it continuously corrects the value of velocity; c_1 and c_2 are termed as cognition and social components respectively are the acceleration constants which changes the velocity of a particle towards $p_{i,p_{\text{best}}}^n$ and $p_{g_{\text{best}}}^n$, (generally somewhere between $p_{i,p_{\text{best}}}^n$ and $p_{g_{\text{best}}}^n$) [60]; r_1^n and r_2^n are two random numbers uniformly distributed in [0,1]; $p_{g_{\text{best}}}^n$ is the best position in the current swarm over generation n determined by the fitness function; and $p_{i,p_{\text{best}}}^n$ is the best position of particle i over generation n determined by the fitness function. A complete description and more details of PSO can be found at a number of publications [60–65]. Herein, only the basic principles were briefly presented.

An opposite representation and fitness function (f) appear to be necessary before the PSO is utilized to train the connectionist network model. Herein, neural network fitness was decided to be the mean square of errors (MSE) of the whole training data set [66]:

$$f = \frac{1}{N}\sum_{i=1}^{N}\left(y_i^{\text{exp}} - y_i^{\text{pre}}\right)^2 \tag{21}$$

where N represents the total number of training data points (input and output pairs), y_i^{exp} is the actual (experimental) at the sampling point i, y_i^{pre} is the ith output of the network. Every particle characterizes a possible solution to the optimization case. As biased of a trained neural network and the corresponding weights are counted a solution, one comprehensive network is represented by a single particle.

Each component of a particle's position vector represents one neural network weight or bias [54]. When the pre-specified criterion is reached, the iterations cease and the set of these optimized weights and biases found is finalized and used in the proposed architecture (see Fig. 3). The detailed flowcharts of the implementations of PSO algorithm for training the proposed ANN architecture are shown in Fig. 4.

4.1.3. ANN structure

Network structure is another important issue that needs consideration due to its considerable impacts on the estimated values. The number of input and output neurons corresponds to the number of input and output data, respectively (8 and 1 in this study). However, the most favorable numbers of hidden layers and neurons in each separate layer are entirely dependent on the complexity of the problem being solved by the neural network and there is no a straightforward scheme to obtain these parameters.

Hornik et al. showed that multilayer feed forward neural networks consist of only one hidden layer with enough number of hidden neurons can map any input to each output to an arbitrary degree of accuracy [67]. Based on the above, in the current study only networks with one hidden layer was examined. In order to find optimum number of neurons, different $2-x-1$ architectures (x varies from 1 to 10) were investigated.

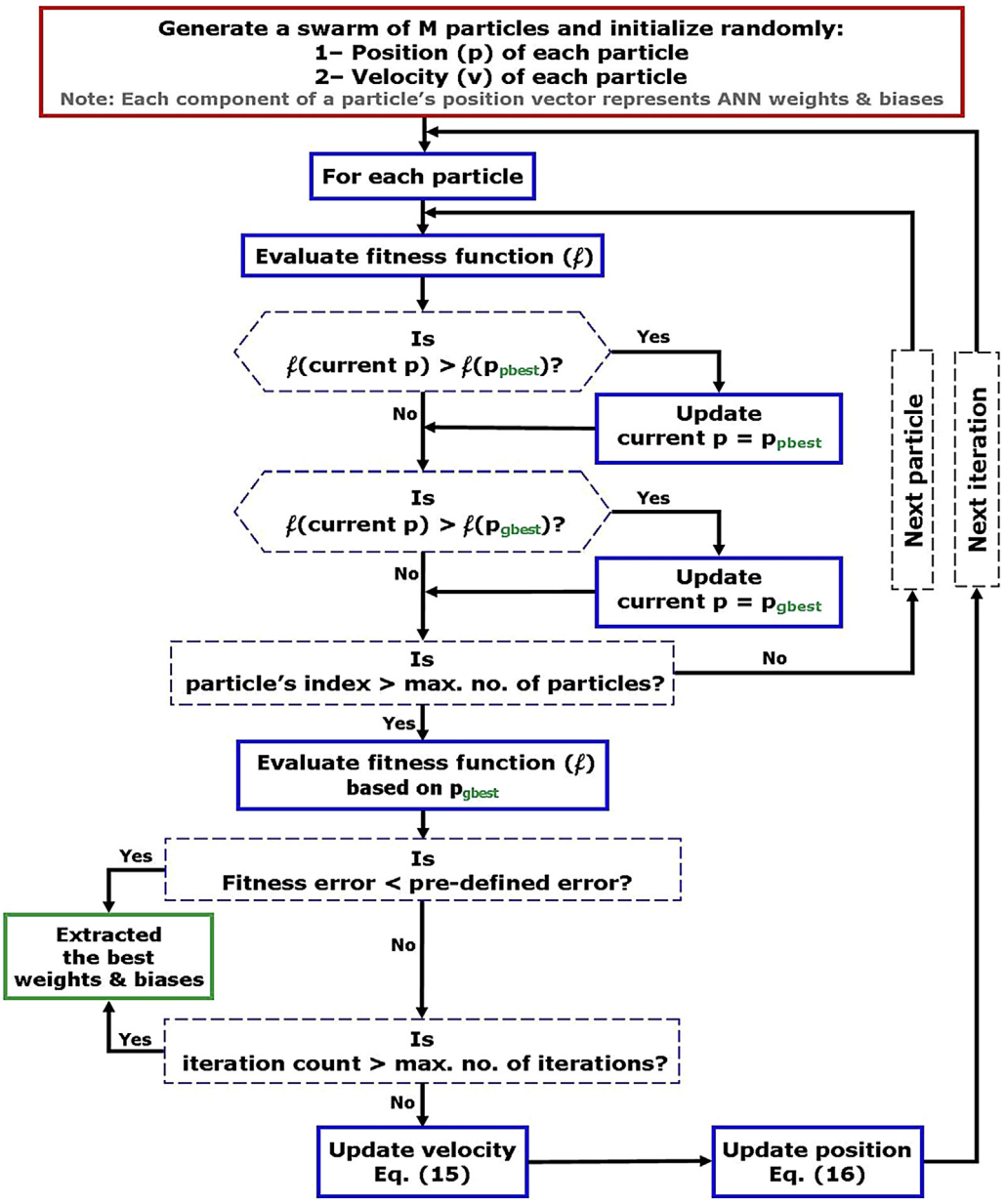

Fig. 4. Flowchart of PSO-based optimization algorithm for evolving the weights and biases of the constructed ANN.

MSE and R^2 values evaluated for different neural network configurations of varying number of neurons in the hidden layer are shown in Fig. 5.

The best configuration for the smart system is normally determined based on the minimum value of MSE and maximum magnitude of R^2. As Fig. 5 depicts, the most appropriate ANN model consists of eight hidden neurons in one layer. Thus, it is found that a three-layer network with a 2 – 8 – 1 different processing stages is the best structure. The final trained ANN model with 8 hidden neurons is shown in Fig. 3.

Table 2 presents the adjustable parameters for the proposed hybrid PSO–ANN approach.

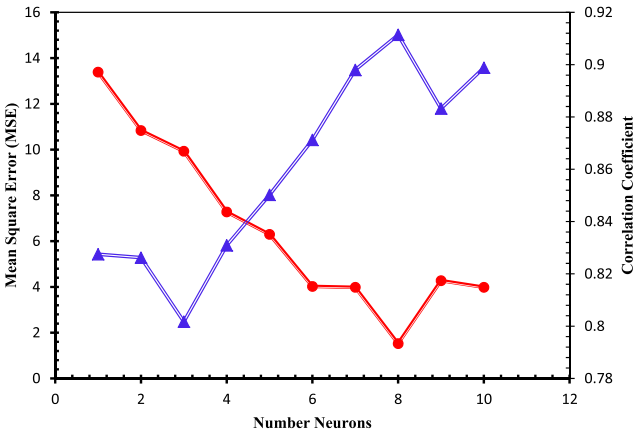

Fig. 5. Effect of number of hidden neurons on performance of the PSO–ANN model in terms of R^2 and MSE values.

4.2. LSSVM model

4.2.1. Data distribution (training and testing subsets)

Like ANNs, for the LSSVM based-model analyses, the database is broken down into training and testing subsets. The training

Table 2
Details of trained ANNs with PSO for the prediction of pseudo-skin factor.

Type	Value/comment
Input layer	2
Hidden layer	8
Output layer	1
Hidden layer activation function	Logsig
Output layer activation function	Purelin
Number of data used for training	96
Number of data used for testing	24
Number of max iterations	500
c_1 and c_2 in Eq. (15)	2
Number of particles	20

data are used for developing the model involves determining of parameters embedded in the LSSVM model. The testing data are used to measure the performance of the model and consequently to evaluate the precision and the effectiveness of the trained LSSVM model on data that play no role in building it. For the analysis, out of 120 data points, 96 data sets are taken for the training process and the rest of the data sets are used for testing the predictive capability of the model.

4.2.2. Kernel function

It is important to choose an appropriate kernel function. There are many types of kernels; however, three typical choices for the kernel function are:

- $K(x,x_k) = x_k^T x$ (Linear kernel)
- $K(x,x_k) = (\tau + x_k^T x)^d$ (Polynomial kernel of degree d)
- $K(x,x_k) = \exp(-x - x_k^2/\sigma^2)$ (Radial basis function RBF kernel)

Entire magnitudes of σ and positive extents of τ meet the Mercer condition [43]. There are many studies in the literature which have made comparisons between the most common kernels [45–47,43]. Provided nonlinear function prediction and nonlinear modeling cases, one can safely apply the RBF kernel as it is an effective way that can produce accurate results [45–47,49,68,48]. Based on the above, this study employed the radial basis function (RBF) as a kernel function.

4.2.3. Optimization method to tune the embedded parameters (γ and σ^2)

It is required to obtain the optimum values of kernel and regularization parameters through the training stage of the LSSVM technique. One effective way to conduct this task is linking the LSSVM model to genetic algorithm (GA) technique which is employed in this study. Indeed, GA which has been initially developed by Holland [69] is recognized as a strong evolutionary algorithm to optimize Kernel RBF parameter (σ^2) and regularization parameter (γ). This tool can be properly designed to handle a variety of optimization problems in the context of biological processes. GA operates with a collection of candidate solutions, called a population.

The system guides the candidate solutions towards an optimum using the principles of evolution and natural genetics. As the search process advances, the population incorporates better and better individuals, and ultimately the convergence is attained, revealing that a single solution defeats it [69]. There are three key operators including mutation, selection, and crossover utilized at every generation of the GA model. It should be mentioned that a chromosome corresponds to a solution vector in GA. An extensive information on GA is found in the literature [65,61,69–72].

The flowchart of GA-based LSSVM incorporating to tune γ and σ^2 values is shown in Fig. 6. It should be noted that the hybridization of LSSVM method with GA had already given encouraging results for various applications [45–48]. The hybrid GA–LSSVM model searching mechanism for optimizing γ and σ^2 parameters is briefly described as follows.

a. *Encoding and generating Initial population*: Defining a chromosome or an array of variable values to be optimized. Herein, the chromosome has 2 variables (a two-dimensional optimization problem) given by {γ, σ^2}. Note that, a

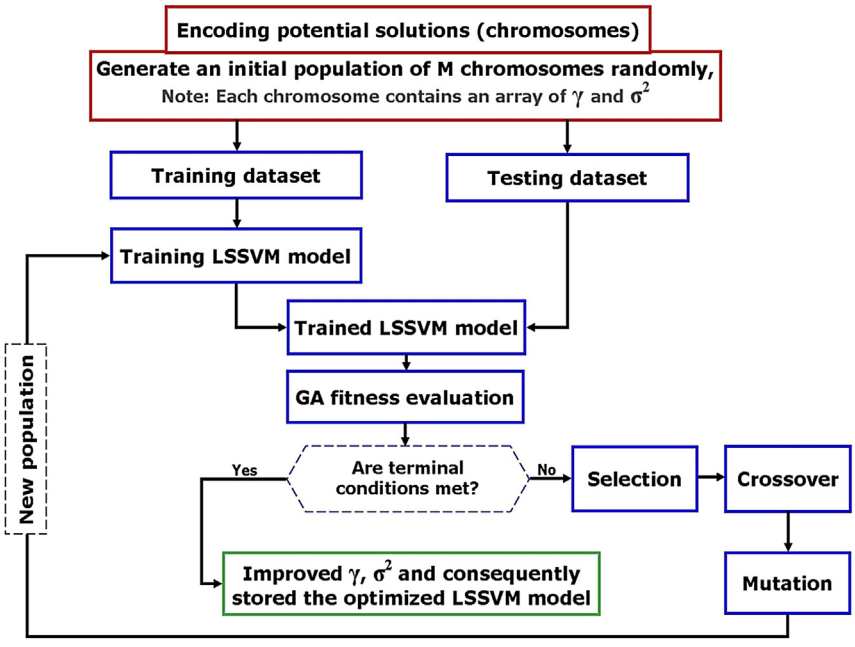

Fig. 6. Flowchart of GA-based optimization algorithm to adjust the embedded parameters of LSSVM model.

chromosome is attributed to a unique solution in the solution space. Therefore, a mapping practice between the chromosomes and the solution space is needed. Encoding is another name for this mapping [69]. After representation of candidate solutions, an initial population of chromosomes was randomly generated.

b. *Fitness assignment*: Evaluate the fitness of each chromosome in the population using a fitness function. Herein, the mean squared error of all training data set was established as fitness function.
c. *Selection*: This stage involves repeating the most triumphant individuals available in a population with a rate which is proportional to their relative quality. Indeed, chromosomes with better fitness values have a greater chance of being selected than those having worse fitness values.
d. *Crossover*: Two different solutions are putrefied in this step and then the parts are randomly combined to create new solutions.
e. *Mutation*: The process disturbs a possible solution through a random way.
f. *Replace*: Use new generated population for the next generation.
g. *Stop criterion*: The procedure is continued unless a number of stopping conditions (e.g. when an acceptable solution has been found or the number of generations that the GA is allowed to execute) are satisfied.

According to the hybrid GA–LSSVM developed in the current study, the final magnitudes of γ and σ^2 are determined to be 2,158,321.5215 and 22.210787768, respectively; implying high predictive potential of the model to determine the outputs with reliable and proper precision. Table 3 represents various settings in adjustment of the LSSVM model and GA optimization parameters.

5. Results and discussions

5.1. LSSVM output results

Before launching the outcomes of the developed vector machine model for pseudo skin factor in rectangular drainage area, it is worth to mention that, distributions of the addressed target (pseudo skin factor) versus independent variables such as dimensionless length, $L/2X_e$ and X_e/Y_e are demonstrated in Fig. 7. Fig. 7 depicts the variation of pseudo skin factor versus corresponding dimensionless length at different drainage area for $L/2X_e = 0.2$.

A regression plot between the estimated pseudo skin factor values and the real values are illustrated in Fig. 8. Fig. 8 demonstrates the scatter diagram that compares experimental pseudo skin factor against LSSVM approach solutions. A tight cloud of points about diagonal line ($Y = X$) for training and testing data sets present the high performance of the developed LSSVM approach.

Table 3
Basic parameter values of GA–LSSVM model for the prediction of pseudo-skin factor.

Type	Value/comment
Input layer	2
Output layer	1
Kernel function	RBF kernel function
Number of data used for training	96
Number of data used for testing	24
GA Population size	1000
Max. number of generations	1000
Crossover rate	0.8
Mutation rate	0.02

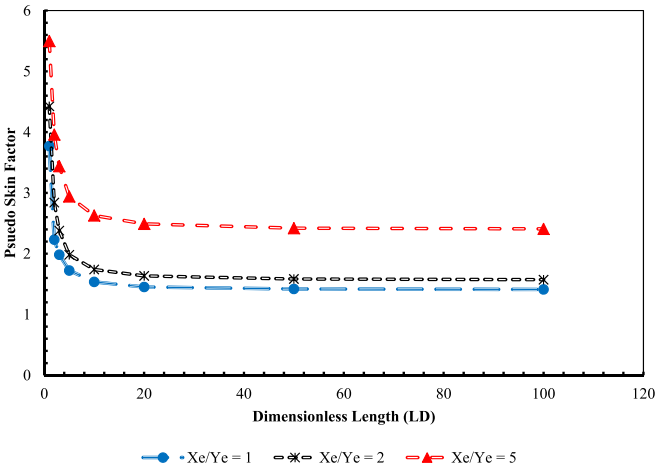

Fig. 7. Variation of skin factor versus dimensionless length (L_D) at different drainage area (X_e/Y_e) for $L/2X_e = 0.2$.

The addressed figure depicts that superior agreement exist between the gained results of LSSVM model and the actual pseudo skin factor in rectangular drainage area. The statistical criteria of the evolved LSSVM approach which includes mean squared errors (MSE), average absolute relative deviations (AARD), and determination coefficients (R^2) are summarized to Table 4.

Fig. 9 depicts the contrast of the measured values of pseudo skin factor and gained outputs of the suggested low parameter model versus corresponding data index. As shown in Fig. 9, the model outputs are reliable because follow exactly the measured pseudo skin factor.

Fig. 10 illustrates the distribution for the deviation of gained outputs applying the LSSVM model versus experimental values of pseudo skin factor for all of the 120 data sets that implemented for developing the LSSVM approach. As demonstrated in Fig. 10, maximum relative deviations of obtained results from corresponding actual skin factor is about ±5%.

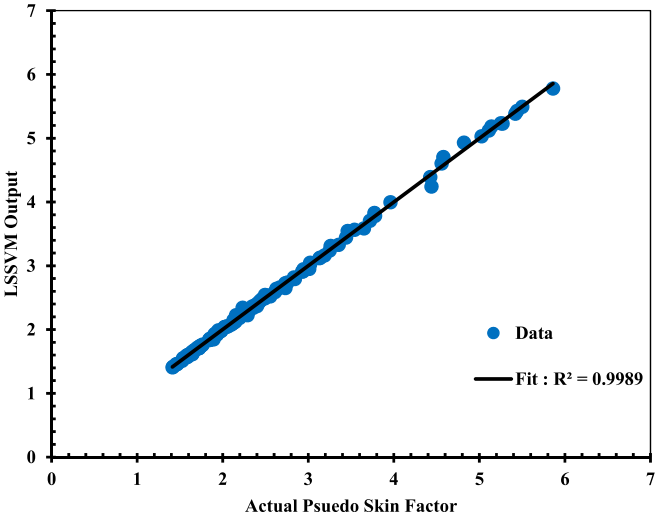

Fig. 8. Regression plot of the proposed vector machine model versus actual pseudo skin factor.

Table 4
Statistical parameters of the evolved LSSVM approach.

Training set	
R^2	0.9988
Average absolute relative deviation	0.77363
Mean square error	0.14151
N	96
Test set	
R^2	0.9991
Average absolute relative deviation	0.98169
Mean square error	0.1445
N	24
Total	
R^2	0.9983
Average absolute relative deviation	0.81524
Mean square error	0.14213
N	120

Moreover, Fig. 11 depicts the comparison between estimated skin factor by utilizing our LSSVM model and actual skin factor versus relevant dimensionless length when $L/2X_e = 1$. As illustrated in Fig. 11, the obtained results from our LSSVM model are matched greatly with corresponding real skin factor for this specific system. In addition, Fig. 12 demonstrates the comparison between estimated skin factor values by LSSVM model and actual skin factor in square drainage area ($X_e/Y_e = 1$) versus relevant dimensionless length (L_D). As shown in Fig. 12, LSSVM result's followed real skin factor values with high level of precision and accuracy.

To determine relative importance of the used input variables on the desired target of this study that is pseudo skin factor, a rigorous statistical method has been implemented. The addressed technique named "analysis of variance (ANOVA)". The obtained materials from the mentioned statistical method are exhibited in Fig. 13. As exhibited in Fig. 13, dimensionless length (L_D) has the highest positive effect on the pseudo skin factor of horizontal wells in the rectangular drainage area.

5.2. PSO–ANN output results

A regression plot between the estimated pseudo skin factor values and the real values are demonstrated in Fig. 14. This figure illustrates the scatter diagram that contrasts real pseudo skin factor against LSSVM approach solutions. A tight cloud of points about diagonal line ($Y = X$) for training and testing data sets present the high performance of the developed LSSVM approach.

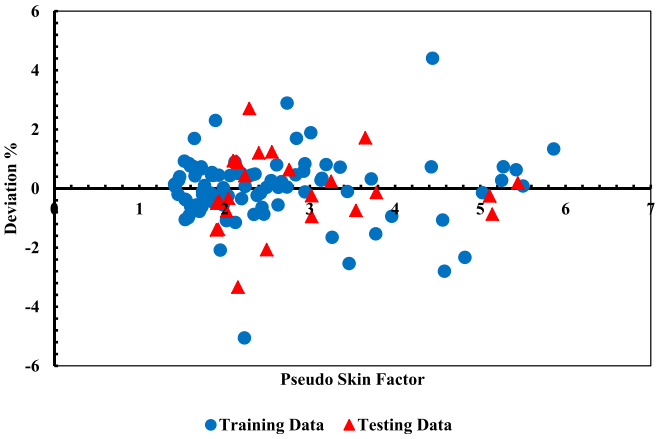

Fig. 10. Relative error distribution of the obtained outputs from LSSVM model versus corresponding pseudo skin factor data points.

The addressed figure depicts that superior agreement exist between the gained results of LSSVM model and the actual pseudo skin factor in rectangular drainage area. Fig. 15 depicts the contrast of the measured values of pseudo skin factor and gained outputs of the suggested hybridized model versus corresponding data index. As shown in Fig. 15, the model outputs aren't reliable in all boundaries because correlation coefficient between measured pseudo skin factor and PSO–ANN results is much lower than suggested LSSVM model.

Fig. 16 illustrates the distribution for the deviation of gained outputs applying the PSO–ANN model versus experimental values of pseudo skin factor for all of the 120 data sets that implemented for developing the PSO–ANN approach. As demonstrated in Fig. 16, maximum relative deviations of obtained results from corresponding actual skin factor is about ±30% that is not acceptable for engineering applications.

Moreover, Fig. 17 depicts the comparison between estimated skin factor by utilizing our PSO–ANN model and real skin factor versus relevant dimensionless length when $L/2X_e = 1$. As illustrated in Fig. 16, the obtained results from our PSO–ANN model aren't matched precisely with relevant real skin factor for this

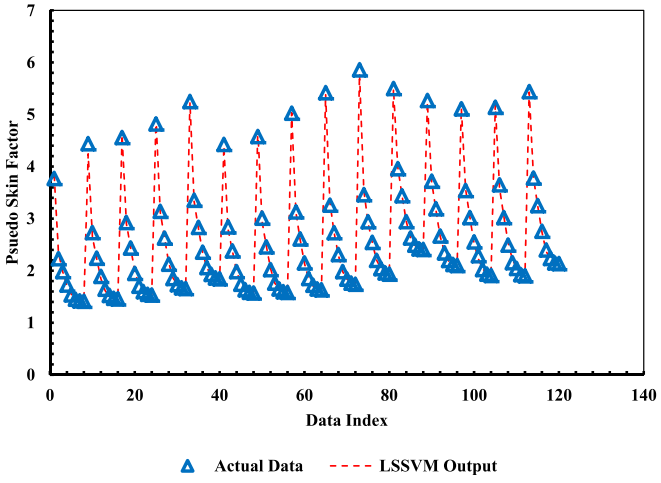

Fig. 9. Comparison between actual pseudo skin factor and predicted values by LSSVM model versus relevant data index.

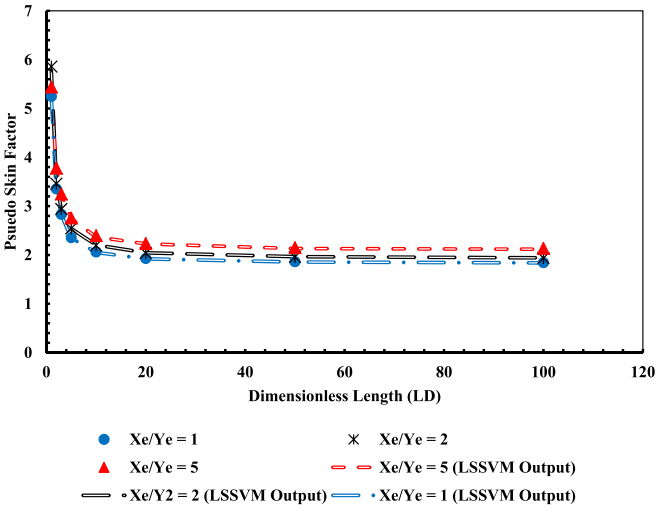

Fig. 11. Comparison between predicted skin factor values by LSSVM model and actual skin factor when $L/2X_e = 1$, versus relevant dimensionless length (L_D).

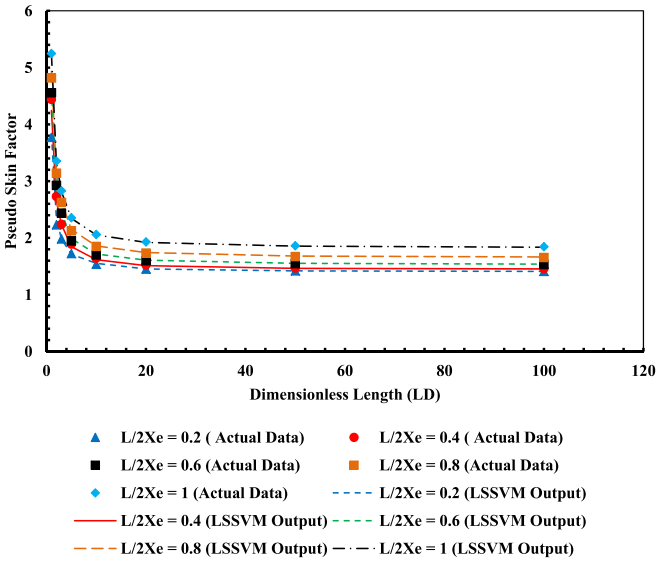

Fig. 12. Comparison between predicted skin factor values by LSSVM model and actual skin factor in square drainage area ($X_e/Y_e = 1$) versus relevant dimensionless length (L_D).

particular system. Furthermore, Fig. 18 depicts the comparison between estimated skin factor values by PSO–ANN model and real skin factor in square drainage area ($X_e/Y_e = 1$) versus corresponding dimensionless length (L_D).

As shown in Fig. 18, results of PSO–ANN model aren't followed real skin factor values with adequate level of precision and accuracy. Finally, the comparison between statistical criteria of the proposed LSSVM model and PSO–ANN model that contains mean squared errors (MSE), average absolute relative deviations (AARD), and determination coefficients (R^2) are summarized to Table 5. As reported in Table 5, suggested LSSVM approach is robust and effective in contrast with PSO–ANN model in estimation pseudo skin factor of horizontal wells in rectangular drainage area.

5.3. Leverage approach

Determining of the outlier of the mathematical approaches plays a vital role in applicability of the addressed approach in the considered issue. Recognition of outlier means that the data, which are very different from the main points in the data bank, are identified. Hence, it seems vital to assess the real data existing for pseudo skin factor data. Since uncertainties influence

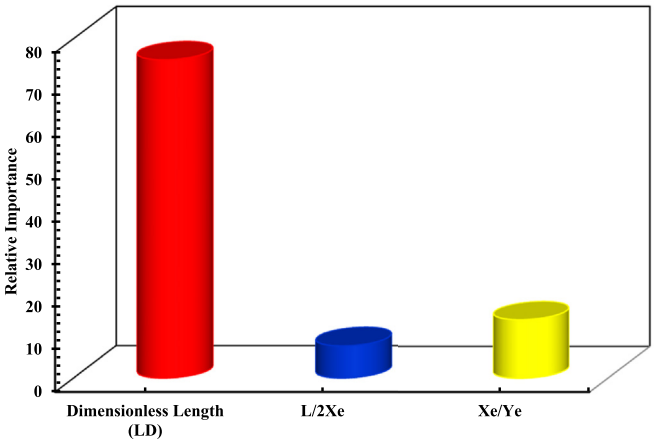

Fig. 13. Relative importance of each input variables on the pseudo skin factor in box shape drainage area.

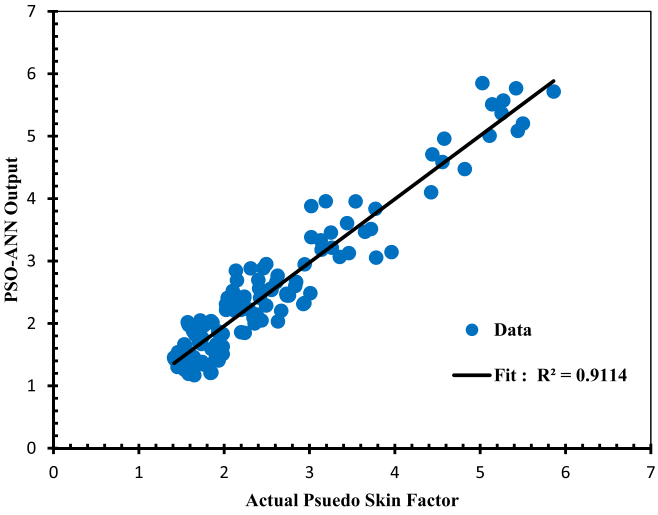

Fig. 14. Regression plot of the proposed PSO–ANN model versus actual pseudo skin factor.

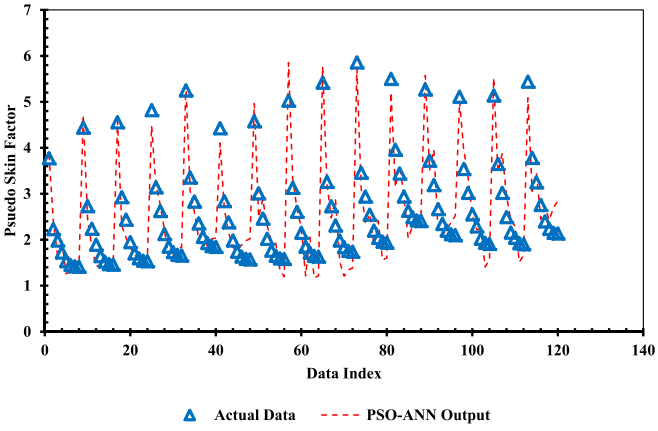

Fig. 15. Comparison between actual pseudo skin factor and predicted values by LSSVM model versus relevant data index.

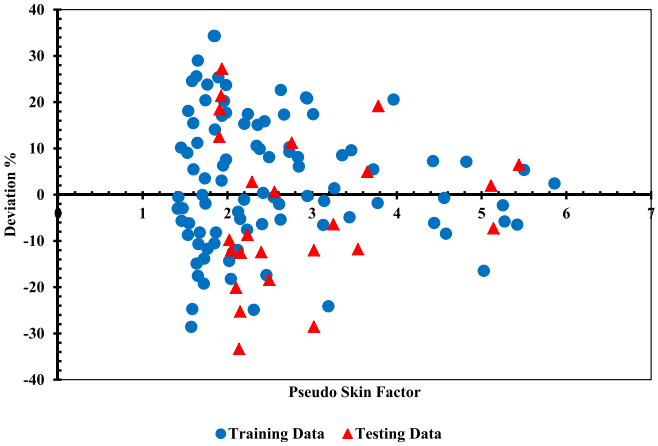

Fig. 16. Relative error distribution of the obtained outputs from PSO–ANN model versus corresponding pseudo skin factor data points.

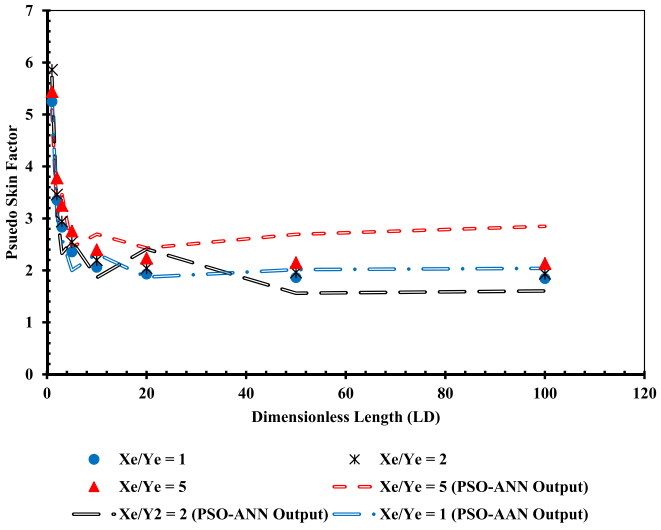

Fig. 17. Comparison between predicted skin factor values by PSO–ANN model and actual skin factor when $L/2X_e = 1$, versus relevant dimensionless length (L_D).

the estimation capability of the evolved approaches. To gain this goal, the approach of Leverage Value Statistics has been carried out. The Graphical discovery of the doubtful data (or outliers) is conducted through theme of the Williams plot owing to the determined H values from the gained outcomes.

A detailed explanation of mathematical backgrounds and computational procedure of this approach can be found in previous literature. The Williams plot is demonstrated in Fig. 19 for the results implementing the vector machine and PSO–ANN approaches. It can be concluded that the developed technique statistically demonstrates high performance in terms of accuracy and applicability range as a large percentage of the data are placed in the intervals H [0, 0.149] and R [−3, 3]. In addition, it

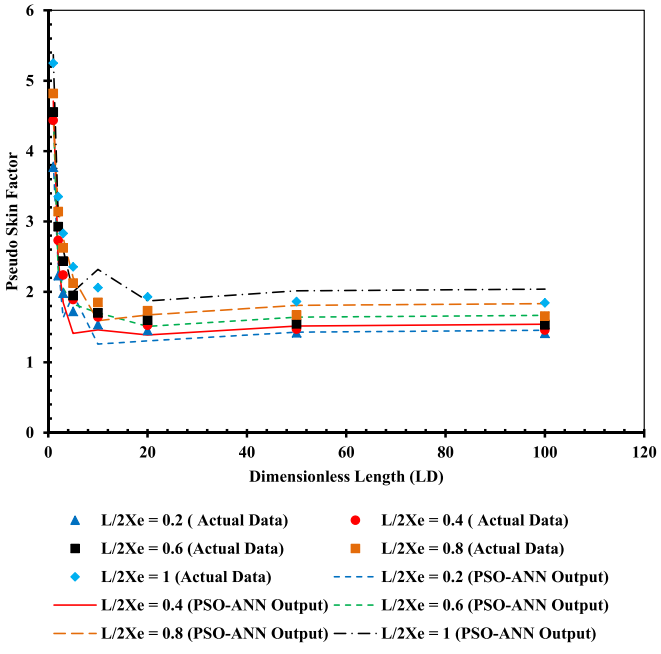

Fig. 18. Comparison between predicted skin factor values by PSO–ANN model and actual skin factor in square drainage area ($X_e/Y_e = 1$) versus relevant dimensionless length (L_D).

Table 5
Calculated statistical indexes of the implemented intelligent based approaches for pseudo skin factor determination.

Statistical parameter	LSSVM	PSO–ANN
(MSE)	0.14213	1.5259
R^2	0.9991	0.9114
AARD	0.81524	12.1011

illustrates that the all data considered for the modeling approach are present within the acceptable ranges.

6. Conclusions

In this paper, an LSSVM model for predicting pseudo skin factor of horizontal wells in the rectangular drainage area has been developed. Through this work massive horizontal well productivities data bank's [1, 21] gathered from literature surveys are faced to the LSSVM model to evolve and examine its robustness. Following deductions can be drawn based on solutions obtained from the LSSVM and PSO–ANN models:

1. Without any doubts at all which having adequate qualitative and quantitative expertise about pseudo skin factor as

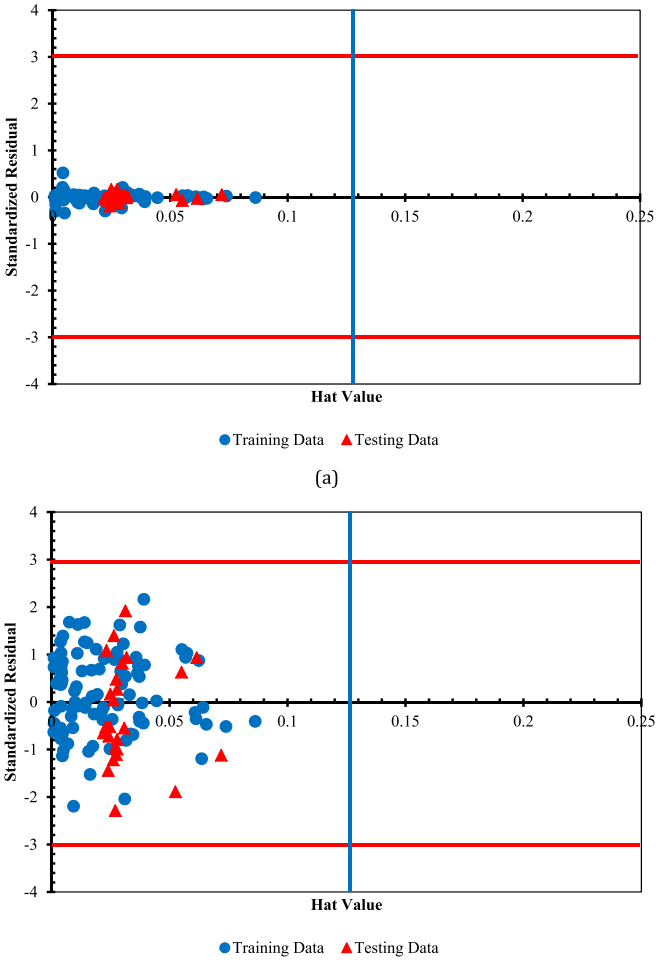

Fig. 19. Detection of the probable doubtful measured skin factor data [1, 21] and the applicability domain of the suggested approaches for the pseudo skin factor. The H^* value is 0.125.

fundamental factor which plays the leading role in productivity of the horizontal wells. In order to gain economic and technical optimizing goals, a numerous number of conventional studies have been done to propose some models for precise calculation of this parameter, but some intrinsic limitations and constraints have triggered attentions to be drawn towards numerical intelligent models.

2. Based on the employed statistical indexes the monitoring of the pseudo skin factor of horizontal wells made by developed LSSVM approach result the closest arrangement with the real data among the artificial neural network approaches.
3. The summary is that performing the evolved approach causes reaching a high degree of performance and precision in terms of calculating the pseudo skin factor of horizontal wells that has not already been conceivable via using conventional schemes.
4. The bottom line of this paper is that the LSSVM model for determining the pseudo skin factor of horizontal wells in box-shaped drainage area is easy-to-use model for petroleum engineers. Moreover, the aforementioned model can couple with commercial reservoir simulators to improve accuracy and decrease run time. Finally, the LSSVM model proposed in this paper can aim the petroleum engineers to determine optimum well location with the concept of reverse engineering.

Nomenclature

Abbreviations

AARD	average absolute relative deviations
ANN	artificial neural network
ANOVA	analysis of variance
BP	back propagation
EOS	equation of state
GA	genetic algorithm
HGAPSO	hybrid genetic algorithm and particle swarm optimization
ICA	imperialist competitive algorithm
LSSVM	least square support vector machine
MAE	mean absolute error (MAE)
MSE	mean squared error (MSE)
PSO	particle swarm optimization
R^2	coefficient of determination
RBF	radial basis function
UPSO	unified particle swarm optimization

Variables

$\overline{y^{\mathrm{P}}}$	the average of the predicted data
$\overline{y^{\mathrm{T}}}$	the average of the actual data
A	drainage area of horizontal well, ft^2
A	extension of drainage volume of horizontal well in x-direction, ft
A_{f}	area open to flow, ft^2
b	extension of drainage volume of horizontal well in y-direction, ft
b_j	bias
B_{o}	oil formation volume factor, rb/STB
C	unit conversion factor
c_1	cognition component
c_2	social components
C_{H}	geometric factor in Babu and Odeh's model
c_{t}	total compressibility, psi^{-1}
D	non-Darcy flow coefficient, day/Mscf
e	error = Actual − Model output
h	reservoir thickness, ft
I_{ani}	permeability anisotropy, dimensionless
J	productivity index, STB/day/psi
K	effective permeability, md
k_{d}	effective permeability in damaged zone, md
k_{H}	horizontal permeability, md
k_{V}	vertical permeability, md
k_x	permeability in x-direction, md
k_y	permeability in y-direction, md
k_z	permeability in z-direction, md
L	horizontal wellbore length, ft
$L_{1/2}$	half-length of horizontal wellbore, ft
L_{D}	dimensionless length
N	the total number of data points
o_j	output
p	reservoir pressure, psi
p_0	reference pressure, psi
p_{avg}	average reservoir pressure, psi
p_{e}	reservoir pressure at boundary, psi
p_{i}	initial pressure, psi
p_{wf}	bottom-hole flowing pressure, psi
q_{o}	oil production rate, STB/day
r_1^{n} and r_2^{n}	two random numbers
r_{dH}	radius of damaged zone in horizontal direction, ft
r_{e}	radius of outer boundary of the reservoir, ft
r_{w}	wellbore radius, ft
s	skin factor, dimensionless
S_j	sum of interconnection weights
s_{R}	partial penetration skin factor, dimensionless
t	time, h
v_i	velocity of particle i
W_{ji}	interconnection weights in network model
x_0	x coordinate of center of well, ft
x_i	position of particle i
x_{e}	half of drainage area side, ft
y_i^{P}	the ith output of the model
y_i^{T}	the actual at the sampling point i
z_0	z coordinate of center of well, ft
z_{w}	distance of wellbore from the lower boundary, ft

Greek letters

μ	viscosity, cp
μ_{o}	oil viscosity, cp
$\emptyset$	porosity, dimensionless
γ	regularization parameter
δ	absolute relative error
ρ	density, lbm/ft3
σ^2	RBF parameter
φ	activation function
ω	the inertia weight

References

[1] A. Abdelgawad, D. Malekzadeh, Determination of the drainage area of horizontal wells in the presence of vertical wells: effect of reservoir and well parameters, J. Can. Petrol. Technol. 40 (10) (2001) 45–54.

[2] A.U. Chaudhry, Oil Well Testing Handbook, Gulf Professional Publishing, Burlington, Mass, 2004.

[3] R.C. Earlougher Jr., Advances in Well Test Analysis, Henry Doherty Memorial Fund of AIME, New York, 1977, p. 330.

[4] C.A. Ehlig-Economides, H.J. Ramey Jr., Pressure buildup for wells produced at a constant pressure, Soc. Petrol. Eng. J. 21 (1) (1981) 105–114.

[5] M.J. Fetkovich, M.E. Vienot, Shape factors, CA, expressed as a skin, scA, J. Petrol. Technol. 37 (2) (1985) 321–322.

[6] D.W. Peaceman, Discussion of productivity of a horizontal well, SPE Reserv. Eng. 5 (2) (1990) 252–253, 360.

[7] J. Wan, V.R. Penmatcha, S. Arbabi, K. Aziz, Effects of grid systems on predicting horizontal-well productivity, SPE J. 5 (3) (2000) 309–314.
[8] E. Yasar, P.G. Ranjith, D.R. Viete, An experimental investigation into the drilling and physico-mechanical properties of a rock-like brittle material, J. Petrol. Sci. Eng. 76 (3–4) (2011) 185–193.
[9] P.L.P. Wasantha, P.G. Ranjith, J. Zhao, S.S. Shao, G. Permata, Strain rate effect on the mechanical behavior of sandstones with different grain sizes, Rock Mech. Rock Eng. (2015), http://dx.doi.org/10.1007/s00603-014-0688-4.
[10] K. Furui, D. Zhu, A.D. Hill, A rigorous formation damage skin factor and reservoir inflow model for a horizontal well, SPE Prod. Facil. 18 (3) (2003) 151–157 (SPE-84964-PA).
[11] V.R. Penmatcha, K. Aziz, Comprehensive reservoir/wellbore model for horizontal wells, SPE J. 4 (3) (1999) 224–233.
[12] D. Malekzadeh, A. Abdelgawad, Analytical and statistical analyses of pseudo skin factors for horizontal wells, J. Can. Petrol. Technol. 38 (10) (1999) 46–54.
[13] I.V. Voronich, L.A. Gaidukov, N.N. Mikhailov, Fluid filtration to a horizontal well with variation in the parameters of the damage zone, J. Appl. Mech. Tech. Phys. 52 (4) (2011) 608–614, 365.
[14] M.D. Clonts, H.J. Ramey Jr., Pressure transient analysis for wells with horizontal drain holes, in: Paper Presented at SPE California Regional Meeting, 2–4 April, Oakland, California, SPE 15116, 1986.
[15] J. Hagoort, A simplified analytical method for estimating the productivity of a horizontal well producing at constant rate or constant pressure, J. Petrol. Sci. Eng. 64 (2009) 77–87.
[16] F. Daviau, G. Mouronval, G. Bourdarot, P. Curutchet, Pressure analysis for horizontal wells, SPE Form. Eval. 3 (4) (1985) 716–724.
[17] E. Ozkan, R. Raghavan, S.D. Joshi, Horizontal well pressure analysis, SPE Form. Eval. 4 (4) (1989) 567–575.
[18] S.D. Joshi, Horizontal Well Technology, PennWell Pub. Co., Tulsa, Okla, 1991.
[19] J. Lu, D. Tiab, Productivity equations for an off-center partially penetrating vertical well in an anisotropic reservoir, J. Petrol. Sci. Eng. 60 (1) (2008) 18–30.
[20] A.S. Odeh, D.K. Babu, Transient flow behavior of horizontal wells pressure drawdown and buildup analysis, SPE Form. Eval. 5 (1) (1990) 7–15.
[21] F. Zeng, G. Zhao, X. Xu, Transient pressure behaviour under non-Darcy flow formation damage and their combined effect for dual porosity reservoirs, J. Can. Petrol. Technol. 48 (7) (2009) 54–65, 370.
[22] P.A. Goode, R.K.M. Thambynayagam, Pressure drawdown and buildup analysis for horizontal wells in anisotropic media, SPE Form. Eval. 2 (4) (1987) 683–697, 340.
[23] M.W. Helmy, R.A. Wattenbarger, New shape factors for Wells produced at constant pressure, in: SPE Paper 39970 Presented at the 1998 Gas Technology Symposium Held in Calgary, Canada, 1998, pp. 15–18 (March 1998).
[24] D.K. Babu, A.S. Odeh, Productivity of a horizontal well, SPE Reserv. Eng. (1989) 417–421 (November).
[25] P.A. Goode, F.J. Kuchuk, Inflow performance of horizontal wells, SPE Reserv. Eng. (1991) 319–324 (August).
[26] M.W. Helmy, R.A. Wattenbarger, Simplified productivity equations for horizontal wells producing at constant rate and pressure, in: SPE Paper 49090 Presented at the 1998 Annual Technical Conference and Exhibition Held in New Orleans, Louisiana, 1998, pp. 27–30 (September 1998).
[27] J. Hagoort, An analytical model for predicting the productivity of perforated wells, J. Petrol. Sci. Eng. 56 (2007) 199–218.
[28] P.N. Mutalik, S.P. Godbole, S.D. Joshi, Effect of drainage area shapes on horizontal well productivity, in: Paper Presented at the SPE 63rd Annual Technical Conference, Houston, Tex., Oct. 2–5, 1988 (SPE 18301).
[29] A. Bahadori, A. Jamili, S. Zendehboudi, Calculating pseudo-steady-state horizontal oil well productivity in rectangular drainage areas using a simple method, Chem. Eng. Commun. 200 (2013) 1–14.
[30] R.M. Butler, Horizontal Wells for the Recovery of Oil, Gas and Bitumen, Monograph No. 2, Petroleum Society of Canadian Institute of Mining, Metallurgy, and Petroleum, 1994.
[31] M. Tabatabaei, D. Zhu, Generalized inflow performance relationships for horizontal gas wells, J. Nat. Gas Sci. Eng. 2 (2010) 132–142.
[32] S. Zendehboudi, M.A. Ahmadi, A. Bahadori, A. Lohi, A. Elkamel, I. Chatzis, Estimation of breakthrough time for water coning in fractured systems: experimental study and connectionist modeling, AICHE J. 60 (5) (2014) 1905–1919.
[33] M.A. Ahmadi, Connectionist approach estimates gas–oil relative permeability in petroleum reservoirs: application to reservoir simulation, Fuel 140C (2015) 429–439.
[34] M.A. Ahmadi, A. Bahadori, A LSSVM approach for determining well placement and conning phenomena in horizontal wells, Fuel 153 (2015) 276–283.
[35] M.A. Ahmadi, A. Bahadori, A robust modeling tool for estimation of a rheological property of heavy oils, Petrol. Sci. Technol. (2015), http://dx.doi.org/10.1080/10916466.2015.1045983.
[36] A. Ahmadi, A. Ahmadi, Applying a sophisticated approach to predict CO_2 solubility in brines: application to CO_2 sequestration, Int. J. Low-Carbon Technol. (2015), http://dx.doi.org/10.1093/ijlct/ctu034.
[37] M.A. Ahmadi, M. Zahedzadeh, S.R. Shadizadeh, R. Abassi, Connectionist model for predicting minimum gas miscibility pressure: application to gas injection process, Fuel 148 (2015) 202–211.
[38] M.H. Ahmadi, M.A. Ahmadi, A. Sadatsakkak, M. Feidt, Connectionist intelligent model estimates output power and torque of stirling engine, Renew. Sustain. Energy Rev. 50 (2015) 871–883.
[39] M.A. Ahmadi, M. Masoumi, R. Askarinezhad, Evolving smart model to predict combustion front velocity throughout in-situ combustion process employment, Energy Technol. 3 (2015) 128–135.
[40] M.A. Ahmadi, B. Pouladi, Y. Javvi, S. Alfkhani, R. Soleimani, Connectionist technique estimates H_2S solubility in ionic liquids through a low parameter approach, J. Supercrit. Fluids 97 (2015) 81–87.
[41] M.A. Ahmadi, A. Bahadori, S.R. Shadizadeh, A rigorous model to predict the amount of dissolved calcium carbonate concentration through oil field brines: side effect of pressure and temperature, Fuel 139 (2015) 154–159.
[42] V. Vapnik, Statistical Learning Theory, Wiley, New York, 1998.
[43] J.A.K. Suykens, T. Van Gestel, J. De Brabanter, B. De Moor, J. Vandewalle, Least Squares Support Vector Machines, World Scientific, Singapore, 2002.
[44] J.A.K. Suykens, J. Vandewalle, Least squares support vector machine classifiers, Neural Process. Lett. 9 (1999) 293–300.
[45] M.A. Ahmadi, M. Masoumi, R. Askarinezhad, Evolving connectionist model to monitor efficiency of the in-situ combustion process: application to heavy oil recovery, J. Energy Technol. 2 (9–10) (2014) 811–818.
[46] M.A. Ahmadi, M. Ebadi, Evolving smart approach for determination dew point pressure through condensate gas reservoirs, Fuel 117 (Part B) (2014) 1074–1084.
[47] M.A. Ahmadi, M. Ebadi, S.M. Hosseini, Prediction breakthrough time of water coning in the fractured reservoirs by implementing low parameter support vector machine approach, Fuel 117 (2014) 579–589.
[48] H. Fazeli, R. Soleimani, M.A. Ahmadi, R. Badrnezhad, A.H. Mohammadi, Experimental study and modeling of ultrafiltration of refinery effluents, Energy Fuels 27 (2013) 3523–3537.
[49] M.A. Ahmadi, M. Ebadi, P.S. Marghmaleki, M.M. Fouladi, Evolving predictive model to determine condensate-to-gas ratio in retrograded condensate gas reservoirs, Fuel 124C (2014) 241–257.
[50] S. Zendehboudi, M.A. Ahmadi, A. Bahadori, A. Shafiei, T. Babadagli, A developed smart technique to predict minimum miscible pressure—EOR implications, Can. J. Chem. Eng. 91 (2013) 1325–1337.
[51] S. Zendehboudi, L.A. James, A. Bahadori, M.A. Ahmadi, Asphaltene deposition in petroleum reservoirs: dynamic test & connectionist modeling, in: International Symposium of the Society of Core Analysts Held in Napa Valley, California, USA, 16–19 September, 2013, 2013.
[52] M.A. Ahmadi, S.R. Shadizadeh, New approach for prediction of asphaltene precipitation due to natural depletion by using evolutionary algorithm concept, Fuel 102 (2012) 716–723.
[53] S. Zendehboudi, M.A. Ahmadi, L. James, I. Chatzis, Prediction of condensate-to-gas ratio for retrograde gas condensate reservoirs using artificial neural network with particle swarm optimization, Energy Fuels 26 (2012) 3432–3447.
[54] M.A. Ahmadi, M. Ebadi, A. Shokrollahi, S.M.J. Majidi, Evolving artificial neural network and imperialist competitive algorithm for prediction oil flow rate of the reservoir, Appl. Soft Comput. 13 (2013) 1085–1098.
[55] M.A. Ahmadi, M. Golshadi, Neural network based swarm concept for prediction asphaltene precipitation due to natural depletion, J. Petrol. Sci. Eng. 98–99 (2012) 40–49.
[56] M.A. Ahmadi, Neural network based unified particle swarm optimization for prediction of asphaltene precipitation, Fluid Phase Equilibr. 314 (2012) 46–51.
[57] M.A. Ahmadi, S. Zendehboudi, A. Lohi, A. Elkamel, I. Chatzis, Reservoir permeability prediction by neural networks combined with hybrid genetic algorithm and particle swarm optimization, Geophys. Prospect. 61 (2013) 582–598.
[58] S. Zendehboudi, M.A. Ahmadi, O. Mohammadzadeh, A. Bahadori, I. Chatzis, Thermodynamic investigation of asphaltene precipitation during primary oil production: laboratory and smart technique, Ind. Eng. Chem. Res. 52 (2013) 6009–6031.
[59] J. Kennedy, R. Eberhart, Particle swarm optimization, Neural Networks, 1995, in: Proceedings, IEEE International Conference on, vol. 4, Nov/Dec 1995, pp. 1942–1948, http://dx.doi.org/10.1109/ICNN.1995.488968.
[60] J. Kennedy, R. Eberhart, Particle swarm optimization, in: Proc. IEEE Int'l. Conf. on Neural Networks (Perth, Australia), vol. IV, IEEE Service Center, Piscataway, NJ, 1995, pp. 1942–1948.
[61] A.P. Engelbrecht, Computational Intelligence: an Introduction, second ed., John Wiley & Sons: University of Pretoria South Africa, 2007.
[62] J. Kennedy, R.C. Eberhart, Y. Shi, Swarm Intelligence, Morgan Kaufmann Publishers, New York, 2001.
[63] J. Kennedy, The particle swarm: social adaptation of knowledge, in: International Conference on Evolutionary Computation (Indianapolis, Indiana), IEEE Service Center, Piscataway, NJ, 1997, pp. 303–308.
[64] R. Mendes, P. Cortez, M. Rocha, J. Neves, Particle swarms for feed forward neural network training, in: Proceedings of the International Joint Conference on Neural Networks, 2002, pp. 1895–1899.
[65] S.N. Sivanandam, S.N. Deepa, Introduction to Genetic Algorithms, Springer-Verlag, Berlin, Heidelberg, 2008.
[66] M.A. Ahmadi, M. Ebadi, A. Samadi, M.Z. Siuki, Phase equilibrium modeling of clathrate hydrates of carbon dioxide + 1,4-dioxine using intelligent approaches, J. Dispersion Sci. Technol. 36 (2) (2015) 236–244.
[67] K. Hornik, M. Stinchombe, H. White, Multi-layer feed forward networks are universal approximations, Neural Netw. 2 (1989) 359–366.

[68] M.A. Ahmadi, M. Masoumi, R. Kharrat, A.H. Mohammadi, Gas analysis by in situ combustion in heavy oil recovery process: experimental and modeling studies, J. Chem. Eng. Technol. 37 (3) (2014) 1–11.
[69] J.H. Holland, Adaptation in Natural and Artificial Systems, MIT Press, Ann Arbor, 1975.
[70] R.L. Haupt, S.E. Haupt, Practical Genetic Algorithms, second ed., John Wiley & Sons, Inc., 2004.
[71] D.E. Goldberg, Genetic Algorithms in Search, Optimization, and Machine Learning, Addison-Wesley, Reading, MA, 1989.
[72] M. Melanie, An Introduction to Genetic Algorithms, MIT Press, 1999.